Journal of Industrial Technology and Innovation 1(1) (2022) 246557

All-optical Noise-free Circuit using Silicon Nonlinear Kerr Effect Space-Time Distortion Control

K. Ray[1], G. Singh[2], Nhat Truong Pham[3,4], P. Hakaew[5], P. Prabpal[5] and P. Yupapin[5,*]

[1]Amity School of Applied Sciences, Amity University Rajasthan, Jaipur, India

[2]Department of ECE, Malaviya National Institute of Technology Jaipur (MNIT) Jaipur, India

[3]Division of Computational Mechatronics, Institute for Computational Science, Ton Duc Thang University, Ho Chi Minh City, Vietnam

[4]Faculty of Electrical and Electronics Engineering, Ton Duc Thang University, Ho Chi Minh City, Vietnam

[5]Department of Electrical Technology, Sakon Nakhon Technical College, School of Industrial Technology, Institute of Vocational Education Northeastern Region 2, Sakon Nakhon, Thailand

***Corresponding author:** preecha@techsakon.ac.th

https://doi.org/10.55674/snrujiti.v1i1.246557

Received: 30 April 2022	Revised: 10 June 2022	Accepted: 27 June 2022	Available online: 1 July 2022

Abstract

A silicon microring resonator system designed for the optical noise-free circuit consists of a silicon microring with two nanorings at its sides and has the form of a Panda-ring resonator. From which the nonlinear Kerr effect is introduced for space-time distortion control. Firstly, the input light (bright soliton) of 1.50 μm center wavelength fed into the system with suitable parameters. The space signal with three types of noise (white, blue- and pink) fed into the system for manipulation. Secondly, the controlled space-time signals multiplexed into the circuit via the add port, the successive filtering employed for noisy space-time signal filtering. The optimum space-time distortion formed by the space-time uncertainty saturation, where the squeezing of light was produced and the whispering gallery mode obtained. The novelty of this work is the use of the Pandaring circuit successive filtering with the space-time distortion control based on the circuit's nonlinear Kerr effect, which can achieve the optical noise-free circuit requirement. By using the Optiwave and MATLAB programs, the simulation results obtained. Results were plotted in time, frequency, and wavelength domains, respectively. The selected modulation time signal is femtosecond (fs), in which the noisy signals extracted from the resonant successive filtering signals.

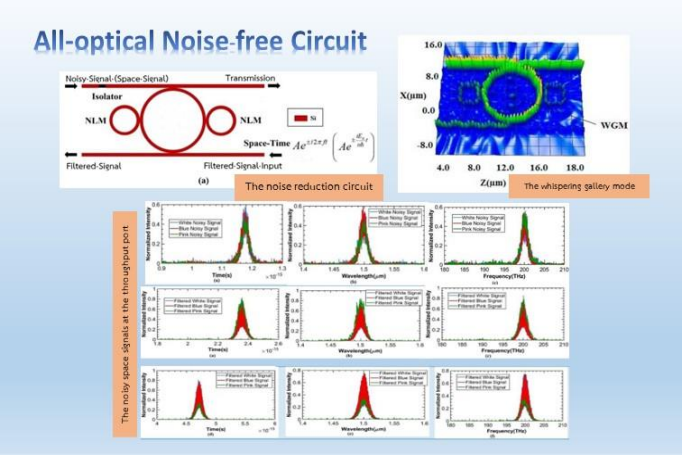

Keywords: Optical noise-free circuit, Silicon microring, Optical noise reduction, Successive filtering, Space-time control

1. Introduction

Noise is any disturbance which usually changes the size or shape of the desired signal, produced within a circuit and as well as at the external sources. In other words, noise interferes and changes the size or shape of the desired signal. They are formed by mechanical vibration, electrochemical- and acoustical feedback [1-4]. Noise reduction is the removal of noise from the signal, where the required noise level can be obtained. Generally, the noise in signal processing devices can be random or white and have even frequency distribution. In a signal processing system, a noise reduction circuit is used to reduce the noise from the signals generated by such a system, which makes use of noise filters. Noise filters are applied to the noise reduction circuits for bad effect reduction, the required clean signals obtained. In other words, the noise filters play a role in maintaining the size or shape of the desired signals when noise removed [5-7]. The noise filters are the key to the noise removal process because without the filters the desired signal will lose its size or shape. There are various types of noise reduction circuits. The radio system has a noise reduction circuit, where the filtering techniques like Butterworth, Chebyshev, and elliptic filters are applied [8-10]. For music systems, the stereo noise reduction circuits are used with filtering techniques similar to that of the radio system. A low-pass filtering technique was applied for radio recording dynamic noise reduction circuit [11-13]. There are other types of noise reduction circuits developed by different researchers [14-16]. Babu et al. [17] developed a noise reduction panel with filter control, where the noise reduction panel has been made from piezoelectric material. The filtering technique involved the canceling the original vibrations of the piezoelectric material by combining this vibration with the source vibrations. This technique reduces the transmitted noise levels. Chang and Jou [18] developed a noise reduction circuit. The circuit consisted of the merging of a low noise amplifier and I/Q mixer. The filtering technique used the dual cross-coupling, which reduces the noise and increases the noise performance of the circuit. Gharibdoust and Bakhtiar [19] proposed a method that reduces noise in an active RC circuit. The method involves using components that are active or passive in the RC circuit, which the noise was reduced. Kubo et al. [20] proposed a noise reduction circuit that used-an acoustic system. The noise reduction circuit consists of a phase-locked loop that is analog and AN (active noise) control circuits. The noise reduction circuit reduces howling in acoustic systems by producing a signal that is opposite in phase to the howling. In this present work, a unique noise reduction scheme for an all-optical noise-free circuit is proposed. The noise reduction circuit consists of a silicon microring with two nanorings at its sides and two linear waveguides. The noise-free circuit using a nonlinear Panda-ring resonator has been employed [21-22]. The successive filtering technique and space-time distortion control have been applied [23-25]. Successive filtering applied to obtain the resonant and stable signals, which involved the number of round trips in a microring circuit. The desired signals are the noise-free output, which are obtained by optimum space-time distortion control. In which the space-time uncertainty saturation is employed. In the simulation, the Optiwave FDTD is used first to simulate the device with the formation of the whispering gallery mode [27-30]. In the second step, the MATLAB program is used to simulate the successive filtering technique with the space-time distortion control, in which simulated parameters are extracted from the

Optiwave FDTD program. The related theoretical background is given. The results plotted and interpreted for the successive filtering and noise- free circuit characteristics.

2. Theoretical Background

In Figure 1(a) and (b) is the schematic and fabrication structure are shown respectively. The noise reduction circuit consists of a silicon substrate, where two silicon linear waveguides and a silicon microring at the center with two nanorings at its sides are present. The bright soliton pulse is selected and used as the space signal given in equation (1) [31] as:

$$E_{in} = B\,\mathrm{Sech}\left(\frac{T}{T_o}\right)^{\left(\frac{z}{2L_D}\right)} \tag{1}$$

where B is the amplitude, z is the propagation distance, T is the propagation time of the soliton pulse. The dispersion $lengthLD = \frac{T_o^2}{\beta}$, where T_o is the initial propagation time, β is the linear and non-linear propagation constant. The space signal (bright soliton) has an input wavelength λ_1 The noises added to the space signal are the white Gaussian noise, blue noise, and pink noise [32], which are given in equations (2) - (4).

The white Gaussian noise signal power spectrum is flat/constant and has a Gaussian distribution profile. It is conventionally written as:

$$S(f) = k, \text{ for all } f \tag{2}$$

where $S(f)$ is the spectral density as a function of frequency and k is a constant. The blue noise signal power spectrum is proportional to its frequency. It was written conventionally as:

$$S(f) = f \tag{3}$$

Pink noise signal power spectrum is inversely proportional to its frequency and conventionally written as:

$$S(f) = \frac{1}{f} \tag{4}$$

The multiplexed space-time filtering signal at the add port is given as:

$$E_{add} = De^{\pm i\omega t}Q(n), \tag{5}$$

where $\omega = 2\pi f$, $f = \frac{c}{\lambda_1}$, ω, f, c are the angular frequency, linear frequency and speed of light in vacuum, respectively. D and t are the amplitude and time, respectively. $\pm$ signs of the exponent term are used for the full-time slot axis. The control time is given by $e^{\pm i\omega t}$ and $t = 0$ for the time domain. Also, $Q(n) = \frac{1}{A}\left(G(n) + G(n-1) + \cdots + G(n) - G(A-1)\right)$, where $Q(n)$ is the average value, A is the window size, G is the space signal, and n is the number of samples. Kerr effect exists through the structure and it can be included in the $n = n_0 + n_2 I = n_0 + n_2 \frac{P}{A_{eff}}$ equation, where n is the refractive index, n_0 is the linear refractive index, n_2 is the nonlinear refractive index, I is the optical intensity, P is the optical power and A_{eff} is the effective core area. The two nanorings at the sides of the silicon

microring act as phase modulators that control the whispering gallery mode at resonance. The output fields are described by equations 6 and 7 [33-34]:

$$E_{th} = m_2 E_{in} + m_3 E_{add}, \quad (6)$$

$$E_{drop} = m_5 E_{add} + m_6 E_{in}, \quad (7)$$

where the constants m_i and the related terms are defined in the given references. Throughput port (E_{th}), drop port (E_{drop}), add port (E_{add}), and input port (E_{in}) are termed accordingly. The successive filtering circuit controlled by the two side ring coupling parameters, from which the nonlinear effects coupled with the center ring can give the resonant output.

The normalized intensities of the system output written as:

$$\frac{I_{th}}{I_{in}} = \left[\frac{E_{th}}{E_{in}}\right]^2, \quad (8)$$

$$\frac{I_{drop}}{I_{in}} = \left[\frac{E_{drop}}{E_{in}}\right]^2. \quad (9)$$

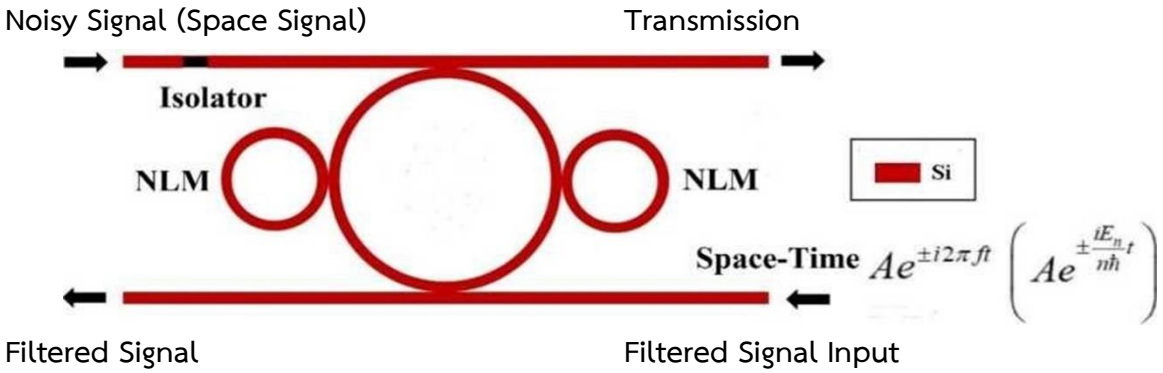

(a)

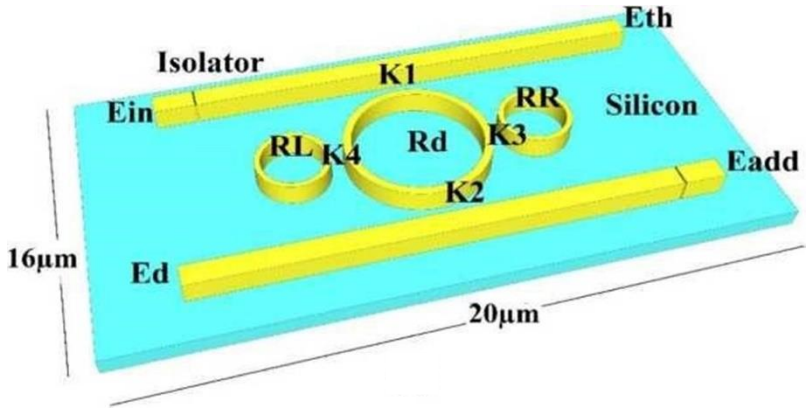

(b)

Figure 1: The schematic diagram is shown in (a), where NLM is the nonlinear phase modulator, (b) a fabrication structure: where the input port, throughput port, add port and drop port are E_{in}, E_{th}, E_{add}, and E_d respectively. Rd : main ring radius, RR and RL : side ring radii, $K1-K4$: coupling constants. The isolator is applied to protect the feedback.

3. Results and Discussion

In the simulation, the 32-bit version 12.0 [35] Optiwave FDTD program is employed as a first step. The simulation model in the Optiwave program has a grid size of 220, 39 and 252 for the three axes (x, y, z), respectively. The APML is the anisotropic perfect matched layer that is employed as the boundary condition. The APML has a layer of 15, a real tensor of 1.0, and a reflection coefficient of 1.0X 10^{-12}. The fabrication structure is shown in Figure 1(b), where the input light from the bright soliton has been fed into the system. The input light has a center wavelength of 1.50 μm, which fed input into the circuit via the input port. The two nanorings at the sides of the silicon center microring act as phase modulators and exhibit the nonlinear effect, which leads to the trapping of light to form the whispering gallery mode. The whispering gallery mode formed at the center ring is shown in Figure 2, where the number of round trips is 20,000 with suitable parameters as described in Table 1. The add-drop filter is the optical filter device that can be applied in all cases. The successive filtering means the running round trips within the same circuit until the resonance and stable, where the selected round trips were 20,000 in this case. The resonant

results are nonlinear due to the ring material itself. Firstly, the Optiwave FDTD program is applied to obtain the results when the nonlinear Kerr nonlinear effect induced into the main ring. Secondly, when the required result is the WGM obtained, the MATLAB program is applied to verify the results with the Optiwave results. From the simulation results of the Optiwave FDTD program, parameters have been extracted. The extracted parameters are used in the MATLAB program. The MATLAB program is employed as a second step in the simulation, from which the successive filtering with the space-time control is simulated. The schematic diagram is shown in Figure 1(a), which is involved in the simulation. The bright soliton multiplexed by white, blue, and pink noises are fed into the system via the input port. At this port, the noisy space signals in the time, wavelength, and frequency domain are obtained as shown in Figure 3, which are induced by the nonlinear Kerr effect.

Figure 3(a) shows the white, blue, and pink noisy signals in the time from 0.9-1.30 fs, respectively. Figure 3(b) shows the wavelength domain for the white, blue, and pink noisy space signals, respectively, with a center wavelength of 1.50 μm. Figure 3(c) shows the white, blue, and pink noisy signals in the frequency domain, respectively, where a peak value is 200 THz. The signal to noise ratio is -0.74 dB (white noise), 0.58 dB (blue noise), 0.58 dB (pink noise). The add port is the second input port, which is employed for modulation and multiplexing operations. The multiplexed signals are input into the added port to employ to space-time control function. The noisy space signals are multiplexed with the time in equation (5), and the description of the system is given in equations (6) and (7). The output is normalized using equations (8) and (9). In this work, the successive filtering of the noisy space signals occurs at the drop port with 50,000 and 100,000 number of round trips. The filtered signals for 50,000 and 100,000 round trips are shown in Figure (4). Figure 4 (a)-(c), shows the filtered white, blue, pink noisy space signal in the time, wavelength, frequency domains for 50,000 round trips, where Figure 4(d)-(f) shows the result of the successive filtering with 100,000 round trips. The signal to noise ratio is 9.55dB (filtered white noise), 9.67 dB (filtered blue noise), and 18.26 dB (filtered pink noise). The filtered signals plotted with space-time projection are shown in Figure 5. By using the 3-interval of time, the filtered white, blue, and pink signals are obtained, respectively. The 50,000 round trip results are shown in Figure 5(a) from -2 to 2 fs, where the two sides of time represent the reverse and forward biased directions, respectively. The 50,000 round trip results are shown in Figure 5(a) from -2 to 2 fs.

The bright soliton is fed into the input port and propagate in the system. The coupling effect from the two side rings introduced the nonlinear coupled with the soliton pulse and chopped the soliton pulse to be the narrower pulse width, which oscillates within the soliton envelop. However, the shorter pulse width gives the power increase due to the shorter time. But the energy conservation maintains as shown in Figures 3 and 4. The coupling power of 3 dB is the general case. However, less coupling power is possible, and the coupling coefficient of 0.06 employed for the simulation with new results obtained as shown in Figures 2-5. The microring Q-factor with a similar scale has been investigated and confirmed by various works [36]. The noisy signals multiplexed with the soliton pulse are shown in Figure 3, introduced by the nonlinear coupling (Kerr effect) between optical power and silicon material. The noisy signals are formed in the circuit and transmitted to the network. In this work, the space-time distortion control has

been applied to extract the noisy signals, which is known as the successive filtering method. From which the filtered signals are obtained with the certain successive round trips shown in Figures 3 and 4. The off-resonance condition is formed by the space-time input via the add port, in which the noise-free signals are obtained. From Figure 5(a) and (b), the noise-free circuit has been achieved when the space-time distortion control is employed. By using the space and time functions in equations (1) and (5), the distortion of space and time control within the circuit in Figure 1 can be applied.

The main point of the noise-free method is the space-time distortion control, where the matching of the two side rings induced by the optical path difference generated by the nonlinear Kerr effect. The optimum value is obtained when space and time uncertainty saturation is achieved when Az. Ap=AF. At~b, from which the squeezed light at the center known as a WGM is obtained. The important is the two side ring parameters, which can lead to having the resonant space-time uncertainty saturation. The space-time distortion can be balanced by the suitable silicon nonlinear effect and optical path differences of the light propagating within the two rings. The space-time uncertainty relationship between Az and at approached 0 being introduced by the stopping condition, i.e., the squeezed state. From which the whispering gallery mode is formed. When the selected modulated signals with the given space and time (frequency) is applied to the add port, the noisy signals disappeared due to off-resonance behavior. It is known as a noise-free circuit condition, which is confirmed by the Rabi oscillation [23]. In this condition, there is no oscillation in time. The noise-free circuit has been obtained, which is free from the noisy signals.

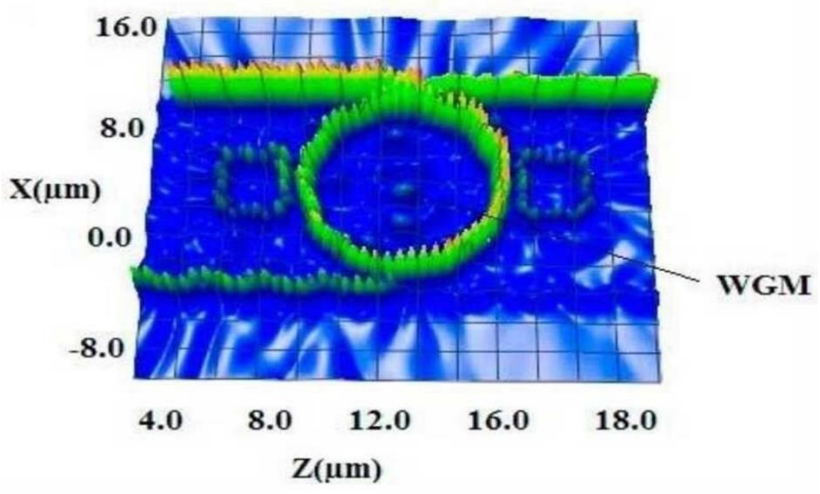

Figure 2: Shows the Optiwave results, where the whispering gallery mode formed at the center ring by using suitable parameters in Table 1.

Table 1: The selected parameters used in simulation.

Parameters	Symbols	Values	Units
Input power (Bright soliton)	P	100	mW
Length of silicon linear waveguide	L	17.0	μm
Silicon center ring radius	Rd	3.0	μm
Left nanoring radius	R_L	1.0	μm
Right nanoring radius	R_R	1.0	μm
Insertion loss	γ	0.5	
Coupling coefficient	κ	0.06	
Refractive index Si [30]	n_{Si}	3.42	
Si nonlinear refractive index [37]	n_2	1.3×10^{-13}	m^2W^{-1}
Input light wavelength	λ_1	1.50	μm
Waveguide core effective [37]	A_{eff}	0.30	μm^2
Waveguide loss	α	0.50	$dB.(cm)^{-1}$

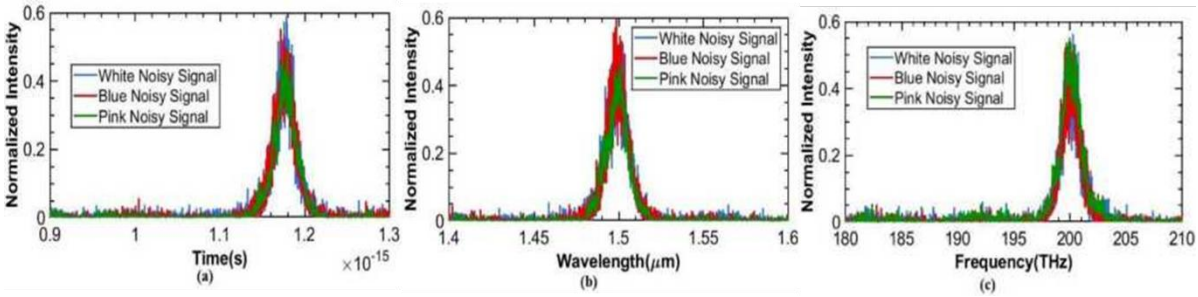

Figure 3: Plot of the noisy space signals at the throughput port where: (a-c) is the white, blue and pink noisy space signal in the time, wavelength and frequency domain respectively. The signal to noise ratio is: -0.74 dB (white noise), 0.58 dB (blue noise), 0.58 dB (pink noise).

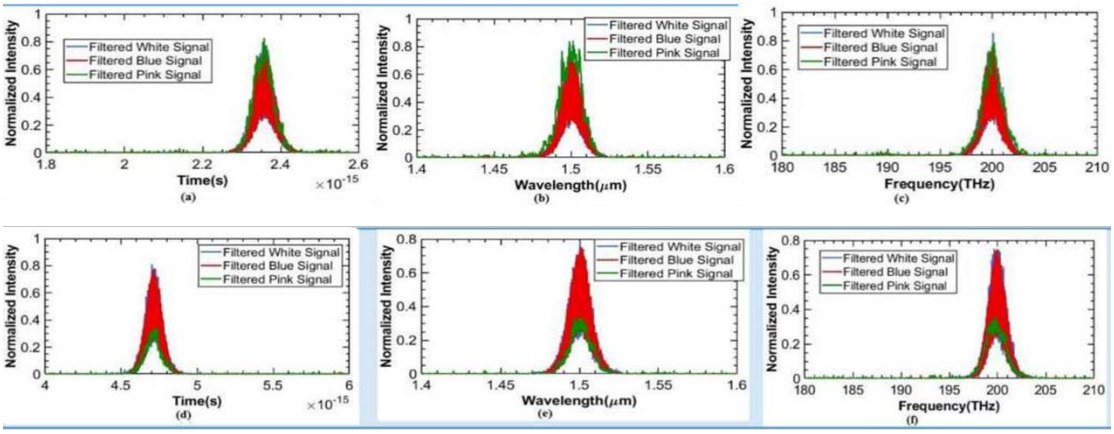

Figure 4: Plot of the filtered signals at the drop port, where (a)-(c) is the filtered white, blue, and pink noisy signal in the time, wavelength, and frequency domain, respectively for the successive filtering round trips of 50,000 of (d)-(f): the filtered white, blue, and pink noisy respecting to in the time, wavelength and frequency domain respectively for 100,000 round trips. The signal to noise ratio is: 9.55 dB (filtered white noise), 9.67 dB (filtered blue noise), and 18.26 dB (filtered pink noise).

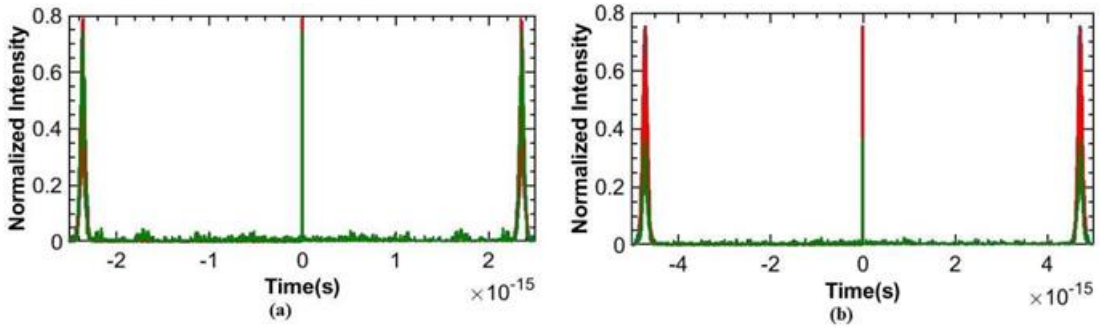

Figure 5: Plot of the filtered signals of the successive filtering and space-time distortion control, where the projection (a) the filtered white, blue- and pink signals, respectively, with 50,000 round trips, while (b) the filtered white, blue and pink signals respectively, with 100,000 round trips.

4. Conclusion

A unique optical noise reduction design and simulation for an all-optical noise-free circuit is proposed in this paper. By a nonlinear Panda-ring, the noise reduction circuit with the space-time distortion control has been formed. The space signal multiplexed by three types of noises (white, blue, and pink) fed into the system and the space-time distortion and successive filtering have been applied. By using the suitable device parameters, the required filtered signals are obtained making use of the successive filtering with space-time distortion control. The noisy space signals are filtered and plotted with the time, wavelength, and frequency domains. From Figure 3, the signal to noise ratio is given as: -0.74dB

(white noise), 0.58 dB (blue noise), 0.58 dB (pink noise) while Figure 4, the signal to noise ratio is given as: 9.55 dB (filtered white noise), 9.67 dB (filtered blue noise), and 18.26 dB (filtered pink noise). The space-time distortion control is obtained and the noise-free circuit has been achieved. A novel way for optical noise reduction application is the use of the Panda-ring circuit successive filtering with the space-time distortion control. By using the off-resonance condition, all forms of noisy signals vanished, the optical noise-free circuit design achieved, which can be applied for optical signal processing in high-speed devices and optical communication networks. The proposed scheme can also apply with the electronic circuit when the electro-optic converter is employed.

Acknowledgement

One of the authors (Dr. P. Hakaew) would like to thank the Department of Electrical Technology, Sakonnakhon Technical College, School of Industrial Technology, Institute of Vocational Education Northeastern Region 2, Sakonnakhon, Thailand for their research facilities.

Conflict of Interest

The authors have declared that this work has no conflict of interest.

References

[1] F. Prebianca, H. A. Albuquerque, M. W. Beims. Describing intrinsic noise in Chua's circuit. Physics Letters A (2018) 2420-2423.

[2] A. Raeesi, H. Rabbani, L. Beygi, S. Zokaee. Discretized Gaussian model for nonlinear noise in elastic optical networks. Optics Communications, 460 (2020) 125002.

[3] Y. Chen, S. Fomel. Random noise attenuation using local signal-and-noise orthogonalization. Geophysics 80, 6 (2015) WD1-WD9.

[4] D. Xile, Z, Caiping, J. Jiuchun. Evaluation of SOC estimation method based on EKF/AEKF under noise interference Energy Procedia 152 (2018) 520-525.

[5] T. Jeong, I. H. Bae, H. S. Moon. Noise filtering via electromagnetically induced transparency. Optics Communications, 383 (2017) 31-35.

[6] L. Luo, J. Sun, B. Huang. A novel feedback active noise control for broadband chaotic noise and random noise Applied Acoustics 116(2017) 229-237.

[7] A.E. Willner, M. R. Chitgarha, O. M. Yilmaz. All-optical signal processing. Journal of Lightwave Technology 32, 4(2014) 660-680.

[8] B. Chen, S. Yu, Y. Yu, R. Guo. Nonlinear active noise control system based on correlated EMD and Chebyshev filter. Mechanical System and Signal Processing 130 (2019) 74-86.

[9] S.N. Yao, T. Collins, P. Jancovic. Hybrid method for designing digital Butterworth filters. Computers and Electrical Engineering 38 (2012) 811-818.

[10] A. Bensky. Short-range Wireless Communication. 3rded (Newnes, Elsevier, 2019).

[11] J. Benesty, J. Chen, Y. Huang. Binaural Noise Reduction in the time domain with a stereo setup. IEEE Transaction on Audio, Speech and Language Processing 19, 8 (2011) 2260-2272.

[12] J. Chen, J. Benesty. On the time-domain widely linear LCMV filter for noise reduction with a stereo system. IEEE Transaction on Audio, Speech and Language Processing 21, 7 (2013) 1343-1354.

[13] K. Simonov, B.C. Hiesmayr. Constraints on the noise in dynamical reduction models. Physics Letters A (2016) 12531255.

[14] H. Zhang, X. Chen, J. Yao, X. Shu, C. Liu. Relative intensity noise reduction with fiber ring resonator. Optics Communications, 429 (2018) 163-165.

[15] A. Awad. Impulse noise reduction in audio signal through multi-stage technique. Engineering Science and Technology, an International Journal 22 (2019) 629-635.

[16] J. Chang, L. Zhu, H. Li, F. Xu, B. Liu, Z. Yang. Noise reduction in Lidar signal using correlation-based EMD combined with soft thresholding and roughness penalty. Optics Communications, 407 (2018) 290-295.

[17] J. Babu, A. Ramacahndran, J. Philip, C. S. Chandran. Development of noise reduction panel using piezoelectric material. Procedia Technology 25 (2016) 1022-1029.

[18] C. H. Chang, C. F. Jou. A direct conversion merged LNA-I/Q-mixer with noise reduction using dual cross coupling for WiMAX/WiBro applications. IEEE Microwave and Wireless Components Letters 22, 1 (2012) 32-34.

[19] K. Gharibdoust, M. S. Bakhtiar. A method for noise reduction in active-RC circuits. IEEE Transactions on Circuits and Systems 58, 12 (2011) 906-910.

[20] M. Kubo, J. Taniguchi, M. Kato. Howling reduction by analog phase-locked loop and active noise control circuits Applied Acoustics 87 (2015) 174-182.

[21] M. Bahadoran, J. Ali, P.P. Yupapin. Ultrafast all-optical switching using signal flow graph for PANDA resonator Applied Optics 52, 12 (2013) 2866-2873.

[22] M. Bahadoran, 1.S. Amiri. Double critical coupled ring resonator-based add-drop filters Journal of Theoretical Physics 13 (2019) 213-220.

[23] A.E. Arumona, I.S. Amiri, G. Singh, P. Yupapin. Full-time slot teleportation using unified space-time function control. Microwave and Optical Technological Letters, Early view: https://doi.org/10.1002/mop.32307.

[24] Z. Tan, J. Sun, Y. Li, W. Ren, T. Li. All optical space-to-time mapping using modal dispersion of multimode fiber. Optics Communications, 389 (2017) 79-84.

[25] M. Bunruangses, P. Youplao, I. S. Amiri, N. Pornsuwancharoen, P. Yupapin. Double vision model using space-time function control within silicon microring system. Silicon (2019) 1-6: DOI: 10.1007/s12633-019-00356-6.

[26] H. Fan, X. Gu, D. Zhou, H. Fan, L. Fan, C. Xia. Confined whispering-gallery mode in silica double-toroid microcavities for optical sensing and trapping. Optics Communications, 434 (2018) 97-103.

[27] T. Kyeong Lee, H. S. Kim, G. Y. Oh, B. H. Lee, D. G. Kim, T. K. Chung, D. McCloskey, J. F. Donegan, Y. W. Choi. Systematic analysis of whispering-gallery modes in planar silicon nitride microdisks. Optics Communications, 322 (2014) 188-197.

[28] H.J. Chen, X.W. Mi. Optomechanical dynamics in detuned whispering-gallery modes cavity. Optics Communications, 285 (2012) 673-679.

[29] S. Punthawanunt, M. S. Aziz, P. Phatharacorn, S.Chiangga, Jalil Ali, P. Yupapin. LiFi cross-connection node model using whispering gallery mode of light in a microring resonator, Microsystem Technologies 24 (2018) 4833-4838.

[30] H. B. N. Trong, Y. C. Chang. Whispering gallery modes in hybrid AU-ZnO microsphere resonators: experimental and theoretical investigations Optical Materials Express 7, 8 (2017) 2962-2967.

[31] G.P. Agrawal. Nonlinear fiber optics: its history and recent progress [Invited]. Journal of Optical Society America B 28, 12 (2011) A1-A10.

[32] H. Zhivomirov. A method for colored noise generation. Romanian Journal of Acoustics and Vibration, XV, 1 (2018) 14-19.

[33] P P Yupapin, N. Pornsuwanchroen, S. Chaiyasoonthorn. Attosecond pulse generation using nonlinear micro ring resonators.Microwave and Optical Technological Letters 50 (2008)3108-3111.

[34] P Prateep, C. Surasak, P. Yupapin. Analytical and simulation of a triple micro whispering gallery mode probe system for a 3D blood flow rate sensor. Applied Optics 55 (2016) 9504-9513.

[35] OptiFDTD Technical Background and Tutorials (Finite Difference Time Domain) Photonics Simulation Software, Version 12.0. http://www.optiwave.com, Searched on 20th Sept, 2019.

[36] P Yupapin, C. Teeka, J. Ali. Nanoscale nonlinear PANDA ring resonator. 1st ed. CRC Press (2012).

[37] A. M. Prabhu, A. Tsay, Z. Han, V. Van. Extreme miniaturization of silicon add-drop microring filters for VLSI photonics applications IEEE Photonics Journal 2 (2010)436-444.